



Tidal modulation of continuous nonvolcanic seismic tremor in the Chile triple junction region

A. Gallego

Department of Geological Science, University of Florida, Gainesville, Florida, USA

Now at the Department of Geology and Geophysics, University of Hawaii, Honolulu, Hawaii, USA

R. M. Russo

Department of Geological Science, University of Florida, Gainesville, Florida, USA

D. Comte

Departamento de Geofísica, Universidad de Chile, Santiago, Chile

V. Mocanu

Department of Geophysics, University of Bucharest, Bucharest, Romania

R. E. Murdie

CTBTO, Vienna International Centre, Vienna, Austria

Now at St. Ives Gold Mining Company, Kambalda, WA, Australia

J.C. VanDecar

DTM, Carnegie Institution of Washington, Washington, DC, USA

[1] We located continuous seismic tremor with coherent amplitude wave trains in the Chile ridge subduction region ($\sim 46.5^\circ\text{S}$) in two clusters north and south of the Chonos Archipelago, between the Chile trench and the North Patagonian fore arc. Tremor persisted from December 2004 to February 2007 (the entire period of the Chile Ridge Subduction Project temporary seismic deployment), and lasted >17 h on six occasions. Tremor in the more active southern cluster reached a maximum duration of 48 h, and we observed no more than 3 continuous days without tremor activity. The cluster locations coincide with the surface projections of subducted transform faults formed at the Chile ridge. We also detected simultaneous, colocated low-frequency microearthquakes with well-defined impulsive waves within the tremor signals distributed from the surface to 40 km depth, suggesting tremors and earthquakes are part of the same process. The periodicity of tremor duration is strongly correlated with semidiurnal, diurnal, and long-period tides, M₂, N₂, K₁, O₁, P₁, and M_m (12.421 h, 12.000 h, 23.934 h, 25.819 h, 24.066 h, and 27.555 days, respectively). We found a significant correlation between tremor occurrence and Earth tides when tidal stress is calculated for the slip plane of a right-lateral strike-slip fault with strike N 95°E , which is near parallel to subducted transform faults (N 78°E) of the Chile ridge, indicating that the very small stresses resulting from the combination of ocean loading and solid Earth tides (~ 1 kPa) are sufficient to facilitate or suppress tremor production; tremors occur when shear stresses are maximum and wane or are low when shear stresses are minimum.

Components: 7,500 words, 11 figures.

Keywords: nonvolcanic tremor; Chile Triple Junction; tidal modulation; subduction; Nazca Plate; transform fault.

Index Terms: 7230 Satellite geodesy: results (6929, 7215, 7230, 7240); 7240 Transient deformation (6924, 7230, 7240); 7250 Transform faults

Received 6 August 2012; **Revised** 9 January 2013; **Accepted** 8 February 2013; **Published** 16 April 2013.

Gallego, A., R. M. Russo, D. Comte, V. Mocanu, R. E. Murdie, and J. C. VanDecar (2013), Tidal modulation of continuous nonvolcanic seismic tremor in the Chile triple junction region, *Geochem. Geophys. Geosyst.*, 14, 851–863, doi:10.1002/ggge.20091.

1. Introduction

[2] Seismic tremor signals are typically found in volcanic areas and are associated with the underground movement of magma, fluids, or gas [e.g., *Chouet*, 1996]. However, a type of seismic tremor clearly unrelated to volcanic arc activity—termed nonvolcanic tremor (NVT)—has been spatially and temporally correlated with geodetically detected episodes of slow slip in subduction zone fore arcs [*Dragert et al.*, 2001; *Obara*, 2002; *Rogers and Dragert*, 2003; *Obara et al.*, 2004; *Obara and Hirose*, 2006; *Ito et al.*, 2007]. These events were interpreted as episodic unlocking and slow (i.e., weeks) elastic slip of the plate interface, with concomitant fore-arc surface motion, and the tremors were considered to be either a direct manifestation of fluid release due to dehydration of the slab causing cascading ruptures on small fractures [*Obara*, 2002] or shear slip on the plate interface mediated by high pore fluid pressures [*Rogers and Dragert*, 2003; *Shelly et al.*, 2006, 2007a]. Correlation between tremor and solid-lunar tidal variation have been observed in the Japan and Cascadia subduction zones [*Shelly et al.*, 2007b; *Nakata et al.*, 2008; *Rubinstein et al.*, 2008; *Lambert et al.*, 2009] and along segments of the San Andreas fault [*Thomas et al.*, 2009], suggesting that the stresses necessary to trigger tremors are much smaller than stresses involved in earthquake production and that the faults involved are very close to failure. Similarly NVTs were also observed to have been triggered by passage of seismic waves from distant earthquakes [*Rubinstein and Vidale*, 2007; *Gomberg et al.*, 2008; *Peng and Vidale*, 2008; *Peng and Chao*, 2008].

[3] The geometry of the Chile triple junction (CTJ) and Chile ridge (Figure 1) results in the formation of slab windows [*Breitsprecher and Thorkelson*, 2009; *Russo et al.*, 2010b]: as the ridge segments subduct below the South American plate, spreading and seismic slip on subducted transforms continues

[*Murdie et al.*, 1993] without generating a new crust, as mandated by low-pressure and high-temperature upper mantle conditions, opening gaps between the subducted Nazca (NZ) and Antarctic (AN) slabs. The CTJ region appears to have formed the southern limit of coseismic rupture of the great 1960 $M_w = 9.5$ Chile earthquake. One aftershock of this event, the 6 June 1960 M_s 6.9 earthquake, occurred in the CTJ region and was a highly anomalous slow earthquake, which produced a 1.5–2 h wave train of anomalously large-amplitude 10–25 s period Rayleigh waves, lacking associated body wave phases, radiating from a hypocenter along the subducted Taitao transform fault [*Kanamori and Stewart*, 1979].

[4] The occurrence of NVT in Patagonian Chile has been previously reported; tremor was clearly located in the fore arc, almost exclusively north of the CTJ in the Chonos Archipelago [*Gallego*, 2010; *Ide*, 2012]. Here we present results from 2 years of seismic observations of NVT in Patagonian Chile, where the actively spreading Chile ridge subducts beneath South America (Figure 1) [*Russo et al.*, 2010a, 2010b]. We show that NVTs in the CTJ region are associated with motions on Chile ridge transform faults subducted beneath South America. Continued activity of the ridge transforms beneath the fore arc enhances shear failure on adjacent portions of the interplate interface north of the triple junction. Furthermore, we show that shear stresses produced by solid Earth tides and ocean loading enhance tremor activity when they act in a plane oriented parallel to the subducted transform faults.

2. Observation and Tremor Characteristics

[5] In order to identify the tremor signal, we performed a day-by-day visual inspection of vertical component filtered in the 5–15 Hz range. The criteria we used to identify tremor included persistent amplitude of

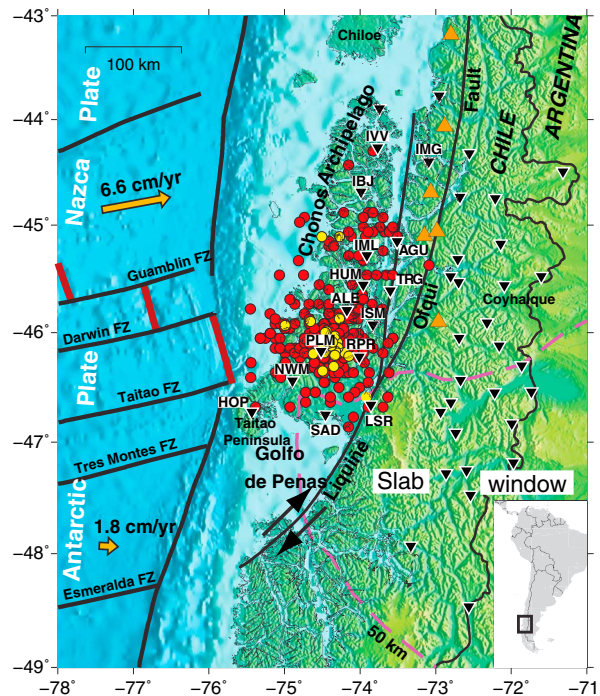


Figure 1. Tectonic setting and seismic network of the study region. Chile ridge spreading centers (heavy red lines). Chile ridge transform faults and fracture zones (heavy solid black lines). Surface projection of slab windows at 50 km depth (dashed purple line) [Russo et al., 2010b]. Holocene volcanoes (orange triangles). NVT locations (red dots). LFE within tremor locations (yellow dots). Seismic sensors (inverted triangles). Plate motions (yellow arrows). The boundary between the Nazca and Antarctic plates is delimited by the ridge and transform fault segments.

long-duration signals above noise, similar wave trains observed nearly simultaneously at more than one station, and correlations of visible tremor burst sequences within the longer tremor wave trains. Start and end times of the tremor signals were selected when that signal was below and above the ambient noise level. Errors in tremor onset and end times are on the order of a few seconds, well below the hourly time series analysis in this study. Cultural noise was not a concern because stations recording tremor were located in the uninhabited Chonos Archipelago.

[6] The CTJ region tremors are long-duration (Figure 2), semicontinuous (100–1000 min) low-frequency (1–10 Hz) seismic signals composed by several bursts (sometimes at regular time intervals; see Figure S1 in the Supporting Information¹), each with a progressive amplitude sequence of increase, maximum, and decay. NVT persisted during 2 years (December 2004 to February 2007) of continuous recording on 15 stations located in the Chonos Archipelago, from a 59 station seismic network, the

¹All Supporting Information may be found in the online version of this article.

Chile Ridge Subduction Project (CRSP), with no more than 3 sequential days without NVT activity. Histograms of NVT occurrence at stations above the subducting Nazca plate (Figure 3) show that stations IBJ and AGU, situated above the subducted Guablin and Darwin fracture zones, recorded minor NVT activity with duration longer than 200 min 5 times. To the south, at stations overlying the subducted Darwin and Taitao FZs, stations HUM, ISM, PLM, RPR, and NWM recorded major activity with durations longer than 1020 min 6 times and a maximum duration of 2880 continuous minutes. However, south of Taitao FZ, where the Antarctic plate subducts, NVT activity at stations HOP and SAD was rare. Particle motions of tremor bursts show that the NVTs are predominantly shear waves (Figure S2). We also observed weak, low-frequency (1–7 Hz) impulsive waves (Figure 4) within tremor signals which show typical separation times (Figure S3) and particle motions (Figure S2) of *P* and *S* waves, similar to low-frequency earthquakes (LFEs) associated with NVT in Japan [Shelly et al., 2006]. Tremor bursts are depleted in high frequencies compared to shear waves of colocated earthquakes (Figure S1).

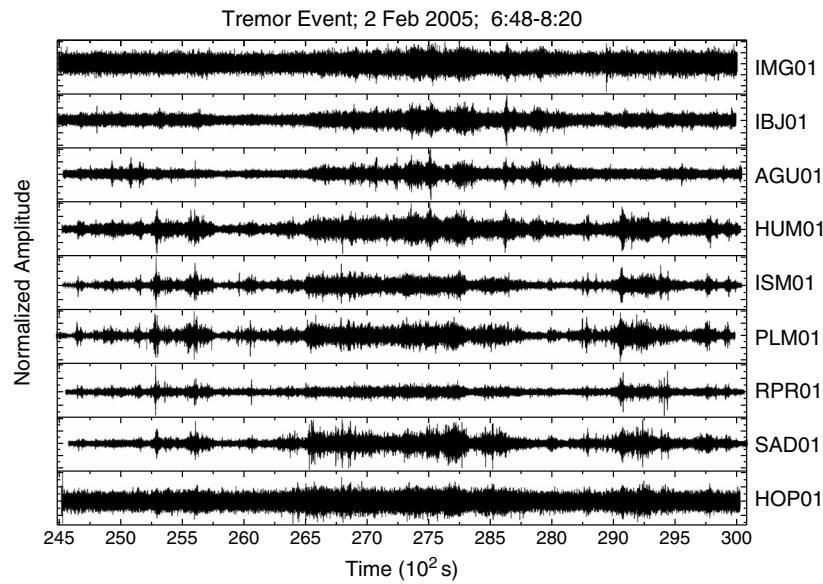


Figure 2. One and a half hours of NVT signal (vertical component) at selected sites. Station names are organized from north to south, IMG being the northernmost and HOP the southernmost.

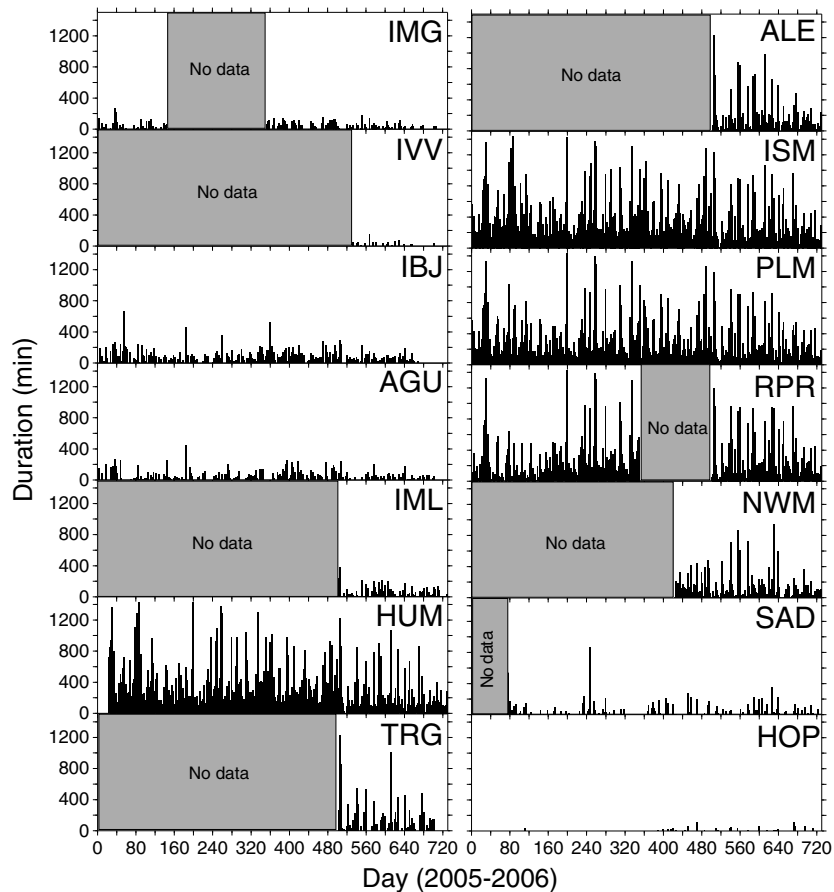


Figure 3. Histograms of tremor occurrence during 2 years of data (2005–2006). Each bar represents activity (in minutes) per day during 2 years of observation. Tremors were detected in stations located in the fore-arc region. Station names are organized from north to south, IMG being the northernmost and HOP the southernmost.

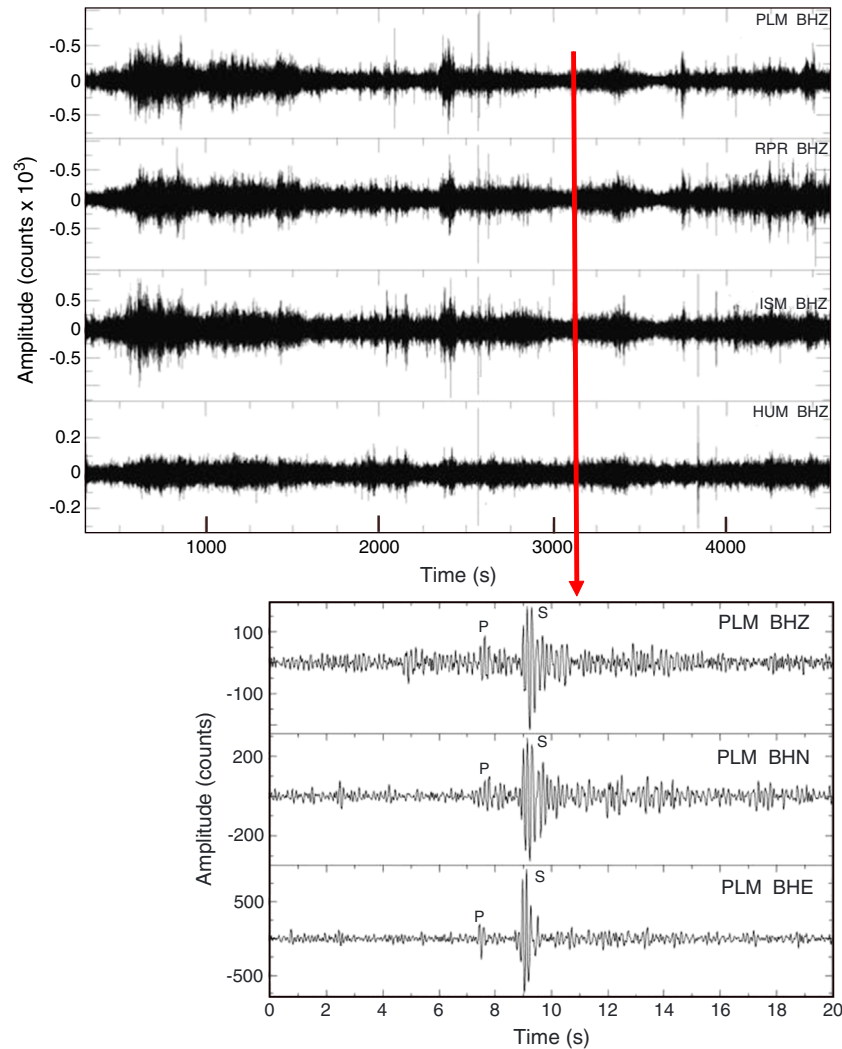


Figure 4. (top) Amplification of a LFE within tremor signals observed at four stations (PLM, RPR, ISM, and HUM) that occurred on 18 July 2005 at 18:11:24. The red arrow indicates the time of the LFE in the raw seismograms. (bottom) Amplified signal representing 20 s of seismogram at station PLM.

3. Tremor Locations

[7] We used timing of tremor bursts recorded at four to eight stations and the source-scanning algorithm (SSA) method of *Kao and Shan* [2004] to locate the tremor signal sources. The study area was parameterized as a grid of 5×5 km cells, using an *S* wave velocity model for the Patagonian Andes [*Robertson et al.*, 2003]. The SSA then yields a tremor burst hypocentral estimate by sequential comparison of the observed and calculated NVT travel times and burst amplitudes between each potential source cell and each station where NVTs were observed. We then used a two-step procedure: In the first step, the signal was visually inspected to find a clear tremor burst. A suitable portion of tremor signal was selected if it contained a relatively high SNR,

duration longer than 20 s, and if it was identified on the same seismometer components (e.g., vertical) at a minimum of four stations. The amplitude of each selected seismogram was then normalized. In the second step, the time window selected was processed through the SSA to calculate the maximum brightness function [*Kao and Shan*, 2004], i.e.,

$$\text{br}(\eta, \tau) = \frac{1}{N} \frac{\sum_{n=-M}^M W_m |u_n(\tau + t_{\eta n} + m\delta t)|}{\sum_{m=-M}^M W_m}$$

where N is the number of stations, $t_{\eta n}$ is the predicted travel time from potential source-cell η to station n , τ is the origin time, u_n is the signal

amplitude at time $t_{\eta m}$, M is the number of samples used to compute the signal amplitude, and δt is the sampling interval. W_m is a weighting factor that depends on how much the predicted signal travel time differs from the observed arrival time. The time window $m\delta t$ selected was 2.5 s. By systematically searching through all n and t in the grid for the local brightness maxima, the spatial and temporal distribution of the tremor source was found (Figure S4). Due to imperfections in the assumed velocity model, the arrival time calculated may differ from the observed time. To calibrate this error, several local earthquakes (LEs) were located using the SSA and compared with the hypocentral estimates derived using HYPO71 location software [Lee and Lahr, 1972], yielding errors of about 10 km horizontally and 30 km vertically. The low-frequency earthquakes found within the tremor signal were located using HYPO71 software when impulsive P and S waves were identifiable.

[8] We located a total of 343 tremors and 27 LFEs. The tremors occurred in the fore arc throughout the region of the Chonos Archipelago, west of the Liquiñe-Ofqui fault zone and the active volcanic arc, and east of the Chile trench (Figure 1). They are distributed in two clusters north of the triple junction whose centers are separated by 125 km. The denser cluster of more active, long-duration tremors is centered on the Taitao Peninsula, almost directly overlying the subducted Taitao transform fault, which is the subducted plate boundary between the Nazca and Antarctic plates, taking up some 5 cm/yr of relative slip. The tremors are distributed in the depth range of 0–90 km, peaking at 30 km depth (Figure S5), and, given poor depth control, may actually lie within the subducted NZ lithosphere and

at or above the interplate contact in the overriding plate. The LFEs are scarce, but the impulsive waves allow more precise source location, demonstrating that tremor bursts and low-frequency earthquakes are collocated to within errors, and simultaneous. LFEs are distributed in the shallowest 60 km peaking at 40 km depth, which is probably a better estimation of tremor depth. The locations thus demonstrate that southern Chile NVTs are not related to the activity of the volcanic arc or the Liquiñe-Ofqui transform fault, which both lie strictly to the east of the tremors.

4. Scale Invariance of Nonvolcanic Tremors

[9] Regression of the time series of cumulative frequency (N) versus tremor duration (T) is better correlated assuming a power law model ($R=0.99$) than an exponential model ($R^2=0.96$) (Figure 5). The calculated linear model using a power law results in

$$\log N = 7.0 - 1.6 \log T \quad \text{with } R = 0.99 \quad (1)$$

[10] Assuming T is proportional to the seismic moment M_0 [Ide et al., 2007]

$$M_0 \approx T \times 10^{12-13} \quad (2)$$

we can express N in terms of M_0 , i.e.,

$$\log N = \alpha - \beta \log M_0 \quad (3)$$

with $\beta=1.6$ and α is some proportional constant. Assuming the relationship between scalar moment and moment magnitude [Hanks and Kanamori, 1979] is

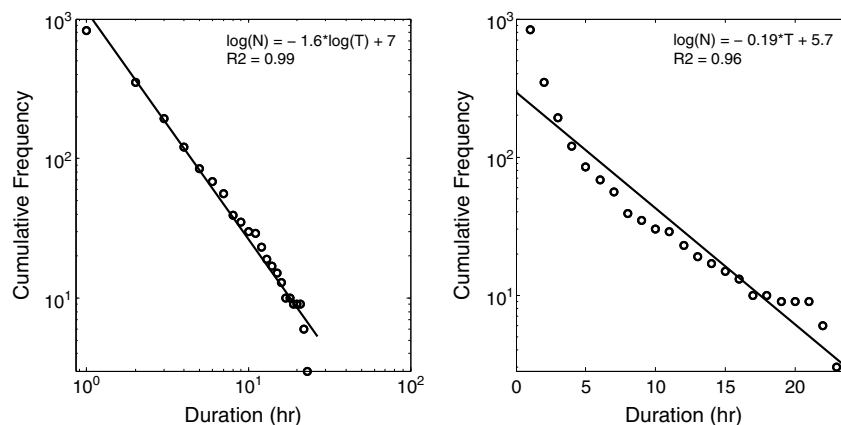


Figure 5. Cumulative frequency of NVT at the Chile triple junction. Number of NVT (N) with duration (T) equal to or greater than x axis time (black circles). The best linear fitting (black line) occurrence for a regression using a power law relation (left) with a correlation coefficient of 0.99. For an exponential model (right), the correlation decreases to 0.96.

$$M_w = \frac{\log M_0}{1.5} - 10.73 \quad (4)$$

yields, in combination with equation (3)

$$\log N = a - bM_w \quad (5)$$

which is similar to the Gutenberg-Richter magnitude-frequency relation for earthquakes [Gutenberg and Richter, 1945], with a b value equal to 2.4. This suggests a scale-invariance pattern similar to that observed for earthquakes and implies that tremor duration depends on stress accumulation. Typical b values for earthquakes are between 0.5 and 1.5 and are attributed to stress conditions and heterogeneities [Frohlich and Davis, 1993]; however, during earthquake swarms or volcanic sequences, that number can increase to 3.6, indicating a larger proportion of smaller than larger events, attributed to high density of cracks and/or high pore pressure [Sánchez et al., 2004].

5. Tremors and Tides

[11] In order to study tidal modulation of NVT activity, we calculated Fourier amplitudes of tremor occurrence time series. Tremor activity detected at two stations (ISM, PLM) on the Taitao Peninsula was binarized (1 during tremor, 0 otherwise) for each hour, 2 years of data yielding 17,520 samples. Southern Chile NVTs are clearly tidally modulated: increased tremor duration/day correlates strongly with peaks of lunar and solar tides M_2 , N_2 , K_2 , K_1 , O_1 , P_1 , and M_m , with periods of 12.421 h, 12.000 h, 11.967 h, 23.934 h, 25.819 h, 24.066 h, and 27.555 days, respectively [Wahr, 1995] (Figure 6). We do not observe the M_f fortnightly lunar (period 13.661 days) or the S_2 semidiurnal (12.658 h) tidal

components, whose expected amplitudes (around 2–3 times that of M_m) suggest that they should be also present. The maximum amplitudes of the tidal constituents vary, but the minimum vertical surface displacement of an observed component (M_m) is small, ~ 21 mm (Table S1). Evolutionary spectrograms of NVT occurrence at stations (Figures 7 and S6) confirm their periodic behavior during the 2 years of data recording, although power at expected tidal periods is much less strong for stations in the north relative to stations proximal to, or on, the Taitao Peninsula. Power spectra also demonstrate that tremor duration correlates positively with the amplitude of the tidal constituent: the greater the tidal displacement (Table S1), the greater the magnitude of the observed peak in power spectrum (Figure 6). Tidal modulation of NVT has been observed in other subduction settings, although only the M_2 and N_2 tidal constituents were detectable [Shelly et al., 2007b; Rubinstein et al., 2008].

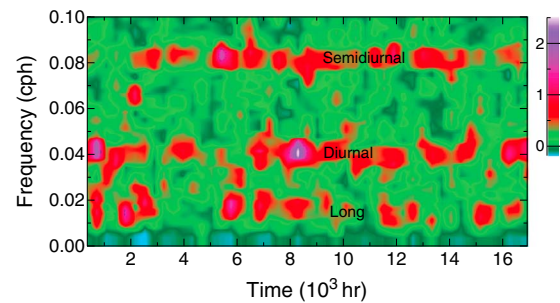


Figure 7. Spectrogram of the PLM station, showing harmonic behavior of tremor occurrence during 2 years (2005–2006) at a 1 h sample interval. The figure shows the high energy at semidiurnal, diurnal, and long-term periods.

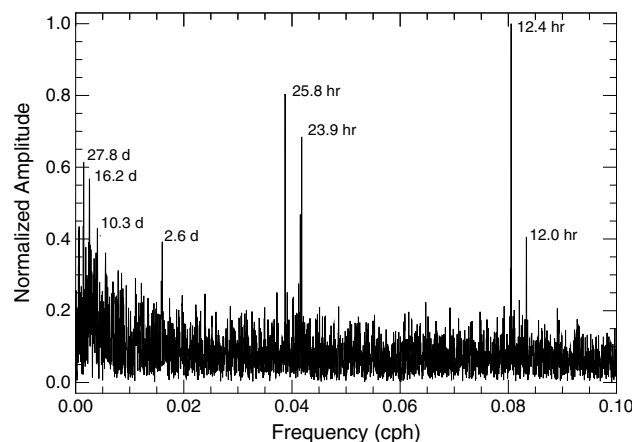


Figure 6. Frequency domain of NVT occurrence for 2 years of data (2005–2006) at a 1 h sample interval. The main cycles correlate with solid Earth tides (Table S1).

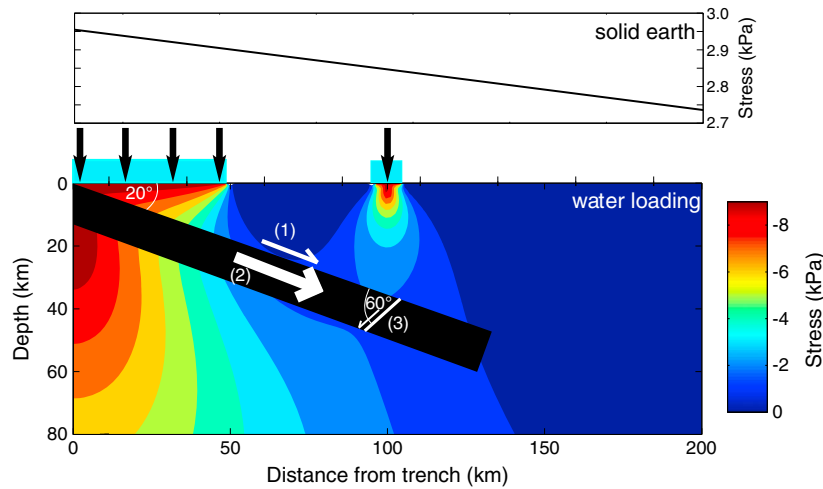


Figure 8. Stress field in the vertical direction (color bar) produced by water loading of the Pacific Ocean and channels of the Chonos Archipelago (blue rectangle). The top curve shows the variation of solid Earth horizontal stress in the E-W direction. Solid Earth and ocean loading stress were calculated for (1) a thrust fault, (2) subducted transform faults, and (3) subducted normal faults.

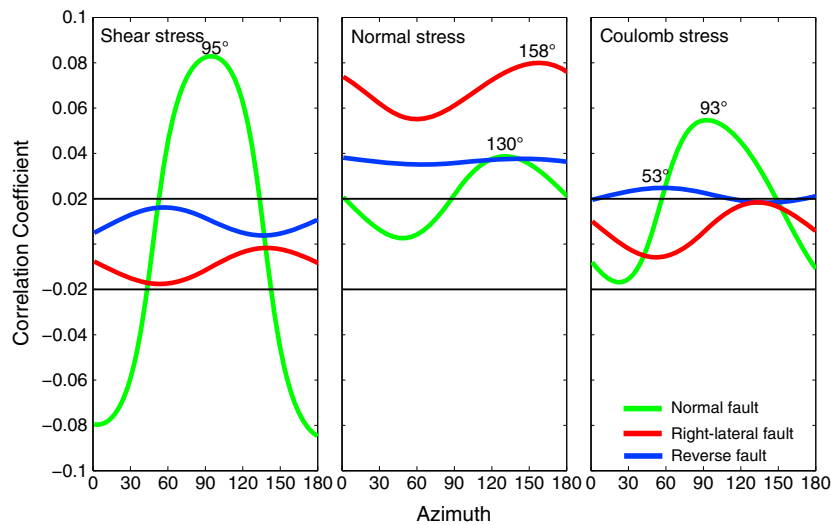


Figure 9. Pearson correlation of 2 years of data between tremor occurrence and shear stress (left panel), normal stress (middle panel), and Coulomb stress (right panel). The correlation was calculated as a function of the strike of a fault plane (azimuth) with dip and rake set for a right lateral (red), reverse (blue) and normal (green) fault as in Figure 8. Numbers in the top of the curves indicate azimuthal angle where correlation is maximum. Correlation is significant at the 99% level for values larger than 0.02.

5.1. Tidal Stresses on Distributed Faults of the Subducted Nazca Plate

[12] Solid Earth tides have been associated with seismicity on shallow faults [Heaton, 1975; Klein, 1976], and earthquake swarms along the Juan de Fuca Ridge [Tolstoy et al., 2002] suggest that faulting occurs when ocean loading is at a minimum, decreasing confining pressure and reducing normal stress. Under certain friction conditions, the projection of the solid Earth tidal stresses in the fault planes of

shallow thrust earthquakes correlates with tidal maxima [Beeler and Lockner, 2003; Cochran et al., 2004]. Faults and fractures in the Nazca plate lithosphere, formed at Chile ridge spreading segments but now in the trench, are clearly observed in high-resolution bathymetry data [Ranero et al., 2006], including normal faults and fractures formed parallel to the overall ridge strike during spreading, and as multiple, complex fault surfaces generally parallel to the overall fault system strike in transform faults that offset ridge segments [Fox and Gallo,

1984; Goud and Karson, 1985; Tebbens et al., 1990; Carbotte and Macdonald, 1994; Escartín et al., 2007] Thus, subducted Chile ridge normal and transforms faults almost certainly include zones of pervasive faulting and fracturing parallel to the overall plate boundary structures (ridge segments and transforms) that can serve as shear slip surfaces and conduits for the kind of high-pressure fluids that appear to play an integral role in the modulation of nonvolcanic tremor by tides.

[13] In order to determine if any of these Nazca plate structures were active during NVT, we determined correlation coefficients between tremor activity and the stresses produced by solid Earth tides and ocean loading. Volumetric and horizontal shear stresses were calculated at the location of the southern tremor cluster in the Chonos Archipelago (46°S, 74.5°W) for 2 years of data (2005–2006), at 1 h sampling using the software SPOTL [Agnew, 2012]. Stresses were calculated at the surface, and we assumed that they are invariant down to 30 km where the occurrence of located tremors is maximum (Figures 8 and S5). To calculate the sea level variation, we used a global model of the oceans with a grid size of 0.125° [Matsumoto et al., 2000]. Vertical and horizontal stresses due to ocean loading were calculated using results for an infinitely long strip load (equation S1). Pacific Ocean loading was calculated assuming a loading strip 100 km wide, and the N-S trending Chonos channel system was modeled as a loading strip 5 km wide (Figure 8).

[14] The Nazca plate lithosphere is characterized by three types of brittle structures (Figures 1 and 8): right-lateral oceanic transform faults and normal faults that formed with the lithosphere at the Chile ridge [Cande and Leslie, 1986], and thrust faults that developed during subduction. To test the tidal effects on these structures, we calculated the shear, normal, and Coulomb stresses along representative right-lateral strike-slip with a vertical plane, normal, and reverse faults for a full range of fault orientations (Figure 8). The significance of the correlation between tremors and stresses was calculated using a Pearson correlation with a 99% level of confidence, i.e., correlation ≥ 0.02 (Figure 9).

[15] The Coulomb failure function (ΔCFF), which is defined by Cocco and Rice (2002), is

$$\Delta CFF = \Delta\tau + \mu(\Delta\sigma_n + \Delta P)$$

where $\Delta\tau$ is the shear stress variation along slip on the fault, $\Delta\sigma_n$ is the normal stress change on the fault, ΔP (assumed here to be 0) is the pore pressure change, and μ (0.5) is the friction coefficient.

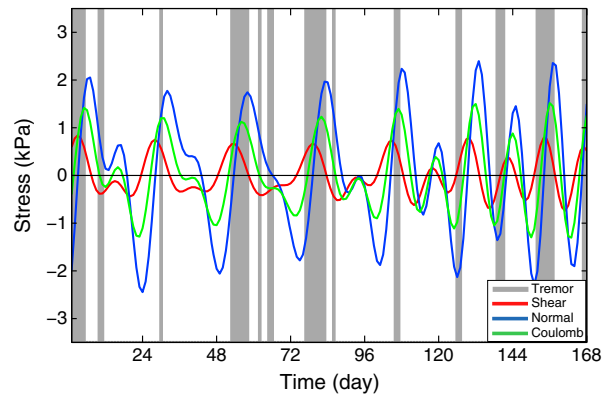


Figure 10. Example of correlation between tremor occurrence (gray bars) and tidal stresses that occurred during 7 days starting on 8 October 2005. (red line) Shear, (blue line) normal, and (green line) Coulomb stresses acting on a fault plane with right-lateral motion oriented N95°E calculated from ocean loading and solid Earth tidal stress (example of the tremor signal for the first 3 days in Figure S7).

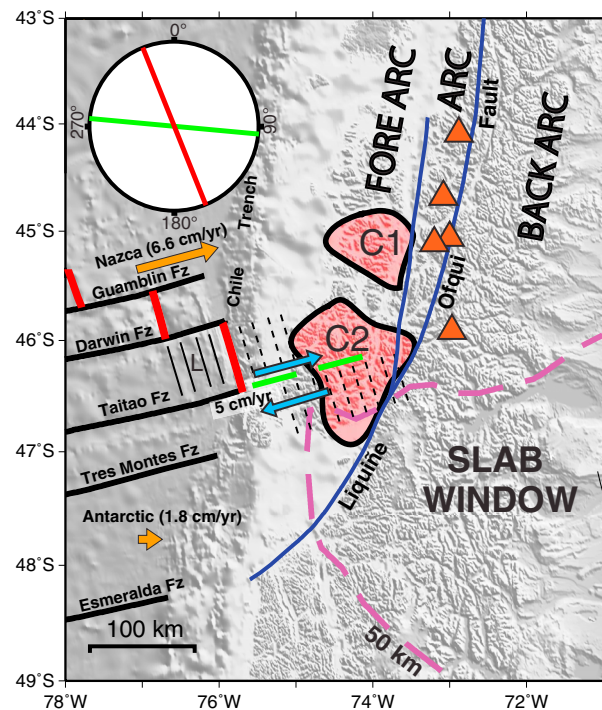


Figure 11. Pole figure (upper left) showing directions of maximum correlation between tremors and tidal shear stress acting on a fault plane with right-lateral (green line) and normal stress acting on a normal fault plane (red line). Nonvolcanic tremors clusters (C1, C2, thick contour lines), fracture zone (solid dark lines), ridge segments (red solid bars), structures associated to ridge segments (solid thin dark lines, L), and interpreted ridge parallel subducted structures (dashed thin dark lines). Relative motion of the Taitao fracture zone (blue arrow). Plate motions (orange arrows). Volcanoes (orange triangles)

[16] The highest observed correlation (0.08) occurs for shear stress acting on right-lateral strike-slip faults striking $N95^{\circ}E$, i.e., subparallel to the subducted Taitao and Darwin transform faults and to the NZ plate convergence direction ($N78^{\circ}E$) (Figure 9). For this type of fault, linear regression shows a coefficient of determination of 0.007, indicating that $\sim 0.7\%$ of tremor occurrence can be explained with a confidence level greater than 99.9% by shear stress acting on the fault. For normal stresses, the maximum correlation (0.08) occurs for normal faults oriented $N158^{\circ}E$, i.e., subparallel to the subducted normal faults ($N168^{\circ}E$) associated with the Chile ridge. The maximum correlation for Coulomb stresses occurs for right-lateral strike-slip faults striking $N93^{\circ}E$, also subparallel to the subducted transform faults. The positive correlation indicates that tremors occur more frequently when shear stresses are positive in the slip direction (Figures 10 and S7).

6. Discussion and Conclusions

[17] Although southern Chile NVTs present many characteristic features of NVT in the Nankai and Cascadia subduction zones (long-duration signals lasting from hours to days, depleted in high frequencies relative to earthquakes, occurring in conjunction with LFEs within the tremor signal, and tidally modulated), there are also important differences: NVTs in the Chile ridge subduction region were nearly continuous, with at most 72 h of quiescence during 2 years of recording, tremors were spatially related to the subduction of the active spreading ridge structures, and they are strongly tidally modulated, correlating with tidal constituents M_2 , N_2 , K_2 , K_1 , O_1 , P_1 , and M_m (Figure 6).

[18] Chilean NVT and LFE lie in a band parallel to the strike of the NZ slab, dispersed within an elongated area of 100 km width, lying 100 km east of the trench (Figure 1). The wide depth distribution of NVT (~ 0 –90 km), with peak of occurrence at 30 km, and depths of LFE within 40 km of the surface (Figure S5) indicate that both phenomena occur mostly near the plate interface and within the overriding South American plate. Two clusters of NVT activity, one very active in the south and another less active in the north, coincide with the locations of Taitao and Darwin subducted oceanic transform faults, respectively, beneath the overriding plate. The subducted dextral Taitao transform fault separates the NZ and AN plates, is the locus of relatively rapid interplate slip at 5 cm/yr, and also generated the very slow M_w 6.9 aftershock of the

great Chile earthquake studies by Kanamori and Stewart [1979]. This anomalous earthquake produced no body waves while generating a 1.5–2 h wave train of anomalously large-amplitude 10–25 s period Rayleigh waves.

[19] The cumulative frequency of Chilean NVT yields a relation similar to the Gutenberg-Richter law with a high b value of 2.4 (Figure 5), indicating a larger proportion of short-duration rather than long-duration events as compared to normal earthquake distributions. High b values have been observed during earthquake swarms [Holtkamp and Brudzinski, 2011] and in volcanic areas [Farrell *et al.*, 2009; Sánchez *et al.*, 2004]. Physical parameters influencing the b value include stress [Scholz, 1968], high pore pressure [Wyss, 1973], and density of cracks [Mogi, 1962]. If tremors are produced by superposition of many low-frequency earthquakes [Shelly *et al.*, 2007b], this result indicates that Chilean tremors are related to the area of the main slip surface, as well as to the volume of fluids and density of cracks along the fault interface. A different result was found in the Tokai Region of Japan [Watanabe *et al.*, 2007], where tremor amplitude and cumulative frequency of tremor duration are exponentially related, possibly as a result of changes in excess fluid pressure or variable stress drop.

[20] In the CTJ area, the correlation between tremor occurrence and soli-lunar tidal variations is maximum when the shear stress produced by the combination of semidiurnal, diurnal, and fortnightly tidal displacements unclamps or enhances shear on existing populations of faults in the NZ plate crust. From linear regression analysis, the highest significant correlation ($R=0.08$) between tremor duration and tides occurs when tidal shear stress acts on the slip plane of a dextral strike-slip fault with a strike near $N95^{\circ}E$ (Figure 11), indicating that at a minimum $\sim 1\%$ of the tremors can be explained by tidally generated dextral shear stress along the Taitao and Darwin transform faults in the Nazca plate, which are loci of both low-magnitude earthquakes [Murdie *et al.*, 1993] and anomalous slow earthquake activity in the wake of megathrusting [Kanamori and Stewart, 1979]. A similar correlation has been observed to occur for shear acting parallel to the San Andreas Fault [Thomas and Nadeau, 2009]. We also found a significant correlation (0.08), for normal stresses in a slip plane oriented $N158^{\circ}E$ with normal motion, i.e., close to the strike of normal faults formed in the subducted Nazca plate at the Chile ridge; however, for other orientations, normal faults show correlations higher than 0.05.

[21] The consistent relationship between the non-episodic Chilean tremors and tidal variation implies that part of NVT activity occurs when tidal stresses attain a threshold value as would be expected if the NVTs were tidally triggered by, for example, changes in Coulomb stress differences [Gomberg *et al.*, 1998; Harris, 1998; Stein *et al.*, 1994], resulting from the combination of ocean loading and solid Earth stresses. The apparent sensitivity of the NVT system to small stresses is consistent with tremors as a manifestation of slip on fault surfaces or fracture surfaces characterized by high density of cracks and high pore fluid pressures, even at the depth of the lower limit of subduction zone locking [Obara, 2002; Rubinstein *et al.*, 2008; Shelly *et al.*, 2007a; Watanabe *et al.*, 2007].

[22] We also observe modulation of the NVT durations at periods of 2.6, 10.3, and 16.2 days (Figure 6), which we interpret as due to periodic infiltration and draining of the complex canal system of the archipelago associated with propagation of trapped water waves in the canals. Periodicity in channelized currents and nearshore trapped Kelvin and shelf waves is observed at the requisite frequencies in the Santa Barbara Channel (6–18 day periods) [Auad and Hendershott, 1997], in Sagami Bay (2.5–7 and >20 day periods) [Kitade *et al.*, 1998], and offshore Honshu, Japan (3–6 day periods) [Kitade and Matsuyama, 2000]. These phenomena appear to be controlled by wind stresses in channels and across continental shelves and by variable remote adjusted sea level due to atmospheric pressure. By analogy, such periods present in NVT from Patagonian Chile are likely related to stress changes caused by periodic loading of the Chonos canals. Direct observations and/or coupled hydrodynamic-elastic modeling required to verify that such water wave phenomena occur in the complex channels of the Chonos Archipelago and could yield the observed long periods in tremor duration are beyond the scope of this paper [Zahel, 1997; Zahel *et al.*, 2000].

Acknowledgments

[23] This work would not have been possible without the help of the following people: Umberto Fuenzalida, Hernan Marilao, Carmen Gloria of the Universidad de Chile; Corporación Nacional Forestal de Chile (CONAF)—Juan Fica, Claudio Manzur, Carlos Llautureo; Sra. Monica Retamal Maturana, Banco Estado; Carabineros de Chile del Region de Aysen; Armada de Chile; Cuerpo Militar de Trabajo del Ejercito de Chile (Cmdte. Roldan, Maj. Wellkner); Alcaldes de Aysen, Melinka (Luis Miranda Chiguay), Rio Ibanez, Lago Verde;

Ejercito de Chile; Aeronautica de Chile (Sr. Carlos Feliu Ruiz); Automotriz Varona (Don Luis Hidalgo); Don Gustavo Lopez y Hostal Bon; Mike Fort, Noel Barstow, Bruce Beaudoin, Jim Fowler of IRIS PASSCAL; Tripulacion de LM Petrel IV (CONAF)—Juan Gallardo, Axel Hernandez, Hernan Aguilar, Jose Geicha Nauto; Gilles Rigaud, Aurelia Rigaud, Valerie Clouard, Lorena Palacio et Morgane; Eduardo Moscoso, Javier; Don Raul Hernandez, Fundo Los Nirres; Ing. Sergio Mirando Contreras (Melinka); Escuela Carlos Condell, Caleta Andrade, Pto. Aguirre (Sr. Victor Figueroa); Enrique Alcalde (Cochrane); Luis Levin (Bahia Murta); Baterias GAMI (Puerto Montt); Mauricio Zambrano L. (Coyhaique Centro de Llamadas); Rolando Burgos and Roselia Delgado, Fachinal; Aladin Jara, Gob. De Chile Chico; Rolando Toloza, Min. Obras Publicas; Mark and Sra. Knipreth, Heart of the Andes Lodge; Tripulacion de El Aleph—Heraldo Zapata Rivera, Ramon Villegas, Omar Tapia Vidal, Jorge Oyarzun Inostroza; Sandalio Munoz, Fundo La Pedregosa; Don Cristian Brautigam; and the many, many people of Region XI, Aysen, who helped us enthusiastically and unstintingly and without whose help this work would have been much less fun. We are grateful to Hayward Oblad and three anonymous reviewers for useful suggestions that strengthened this paper. This work was supported by the U.S. National Science Foundation under Grant EAR-0126244 and CONICYT-CHILE under Grant 1050367.

References

- Agnew, D. C. (2012), *SPOTL: Some Programs for Ocean-Tide Loading*, SIO Technical Report, Scripps Institution of Oceanography
- Auad, G., and M. C. Hendershott (1997), The low-frequency transport in the Santa Barbara Channel: Description and forcing, *Cont. Shelf Res.*, *17*(7), 779–802.
- Beeler, N. M., and D. A. Lockner (2003), Why earthquakes correlate weakly with the solid Earth tides: Effects of periodic stress on the rate and probability of earthquake occurrence, *J. Geophys. Res.*, *108*, 2391.
- Breitsprecher, K., and D. J. Thorkelson (2009), Neogene kinematic history of Nazca-Antarctic-Phoenix slab windows beneath Patagonia and the Antarctic Peninsula, *Tectonophysics*, *464*(1–4), 10–20.
- Cande, S. C., and R. B. Leslie (1986), Late Cenozoic tectonics of the Southern Chile Trench, *J. Geophys. Res.*, *91*(B1), 471–496.
- Carbotte, S. M., and K. C. Macdonald (1994), Comparison of seafloor tectonic fabric at intermediate, fast, and super fast spreading ridges: Influence of spreading rate, plate motions, and ridge segmentation on fault patterns, *J. Geophys. Res.*, *99*(B7), 13609–13631.
- Chouet, B. A. (1996), Long-period volcano seismicity: Its source and use in eruption forecasting, *Nature*, *380*(6572), 309–316.
- Cochran, E. S., J. E. Vidale, and S. Tanaka (2004), Earth tides can trigger shallow thrust fault earthquakes, *Science*, *306*, 1164–1166.
- Dragert, H., K. Wang, and T. S. James (2001), A silent slip event on the deeper Cascadia subduction interface, *Science*, *292*(5521), 1525–1528.
- Escartín, J., S. A. Soule, D. J. Fornari, M. A. Tivey, H. Schouten, and M. R. Perfit (2007), Interplay between faults and lava flows in construction of the upper oceanic crust: The East

- Pacific Rise crest 9°25′–9°58′N, *Geochem. Geophys. Geosyst.*, 8(6), Q06005.
- Farrell, J., S. Husen, and R. B. Smith (2009), Earthquake swarm and *b* value characterization of the Yellowstone volcano-tectonic system, *J. Volcanol. Geoth. Res.* 188, 260–276.
- Fox, P. J., and D. G. Gallo (1984), A tectonic model for ridge-transform-ridge plate boundaries: Implications for the structure of oceanic lithosphere, *Tectonophysics*, 104(3–4), 205–242.
- Frohlich C., and S. D. Davis (1993), Teleseismic *b*-values: Or, much ado about 1.0, *J. Geophys. Res.*, 98(B1): 631–644.
- Gallego, A. (2010), Non volcanic tremors and seismic noise tomography at the Chile triple junction, Ph.D. thesis, Univ. of Florida.
- Gomberg, J., N. M. Beeler, M. L. Blanpied, and P. Bodin (1998), Earthquake triggering by transient and static deformations, *J. Geophys. Res.*, 103(B10), 24411–24426.
- Gomberg, J., J. L. Rubinstein, Z. Peng, K. C. Creager, J. E. Vidale, and P. Bodin (2008), Widespread triggering of nonvolcanic tremor in California, *Science*, 319(5860), 173.
- Goud, M. R., and J. A. Karson (1985), Tectonics of short-offset, slow-slipping transform zones in the FAMOUS area, Mid-Atlantic Ridge, *Mar. Geophys. Res.*, 7(4), 489–514.
- Gutenberg, B., and C. F. Richter (1945), Frequency of earthquakes in California, *Nature*, 156(3960), 371–371.
- Hanks, T. C., and H. Kanamori (1979), A moment magnitude scale, *J. Geophys. Res.*, 84, 2348–2350.
- Harris, R. A. (1998), Introduction to special section: Stress triggers, stress shadows, and implications for seismic hazard, *J. Geophys. Res.*, 103(B10), 24347–24358.
- Heaton, T. H. (1975), Tidal triggering of earthquakes, *Geophys. J. R. Astron. Soc.*, 43(2), 307–326.
- Holtkamp, S. G., and M. R. Brudzinski (2011), Earthquake swarms in circum-Pacific subduction zones, *Earth Planet. Sci. Lett.*, 305(1–2), 215–225.
- Ide, S., G. C. Beroza, D. R. Shelly, and T. Uchide (2007), A scaling law for slow earthquakes, *Nature*, 447(7140), 76–79.
- Ide, S. (2012) Variety and spatial heterogeneity of tectonic tremor worldwide, *J. Geophys. Res.*, 117(B03302), 1–18
- Ito, Y., K. Obara, K. Shiomi, S. Sekine, and H. Hirose (2007), Slow earthquakes coincident with episodic tremors and slow slip events, *Science*, 315(5811), 503–506.
- Kao, H., and S. J. Shan (2004), The source-scanning algorithm: Mapping the distribution of seismic sources in time and space, *Geophys. J. Int.*, 157(2): 589–594.
- Kanamori, H., and G. S. Stewart (1979), Slow earthquake, *Phys. Earth Planet. Inter.*, 18(3), 167–175.
- Kitade, Y., and Matsuyama, M. (2000), Coastal-trapped waves with several-day period caused by wind along the southeast coast of Honshu, Japan, *J. Oceanogr.*, 56(6), 727–744.
- Kitade, Y., M. Matsuyama, S. Iwata, and I. Watabe (1998), SDP and LP fluctuations observed along the coast of Sagami Bay, *J. Oceanogr.*, 54(4), 297–312.
- Klein, F. W. (1976), Earthquake swarms and the semidiurnal solid Earth tide, *Geophys. J. R. Astron. Soc.*, 45(2), 245–295.
- Lambert, A., H. Kao, G. Rogers, and N. Courtier (2009), Correlation of tremor activity with tidal stress in the northern Cascadia subduction zone. *J. Geophys. Res.* 114, doi: 10.1029/2008JB006038
- Lee, W. H. K., and J. C. Lahr (1972), HYP071: A computer program for determining hypocenter, magnitude, and first motion pattern of local earthquakes, Open File Report, U. S. Geological Survey, 100 pp.
- Matsumoto, K., Takanezawa, T., and Ooe, M. (2000), Ocean tide models developed by assimilating TOPEX/Poseidon altimeter data into hydro-dynamical model: A global model and a regional model around Japan, *J. Oceanogr.*, 56, 567–581.
- Mogi, K. (1962), Magnitude-frequency relation for elastic shocks accompanying fractures of various materials and some related problems in earthquakes, *Bull. Earthquake Res. Inst. Univ. Tokyo* 40, 831–853.
- Murdie, R., D. J. Prior, P. Styles, and S. S. Flint (1993), Seismic responses to ridge-transform subduction: Chile triple junction, *Geology*, 21(12), 1095–1098.
- Murthy, V. N. S. (2002), *Geotechnical Engineering: Principles and Practices of Soil Mechanics and Foundation Engineering*, Marcel Dekker Inc., New York, pp. 881–950.
- Nakata, R., N. Suda, and H. Tsuruoka (2008), Non-volcanic tremor resulting from the combined effect of Earth tides and slow slip events, *Nat. Geosci.*, 1(10), 676–678.
- Obara, K. (2002), Nonvolcanic deep tremor associated with subduction in southwest Japan, *Science*, 296(14), 1679–1681.
- Obara, K., and H. Hirose (2006), Non-volcanic deep low-frequency tremors accompanying slow slips in the southwest Japan subduction zone, *Tectonophysics*, 417(1–2), 33–51.
- Obara, K., H. Hirose, F. Yamamizu, and K. Kasahara (2004), Episodic slow slip events accompanied by non-volcanic tremors in southwest Japan subduction zone, *Geophys. Res. Lett.*, 31, L23602.
- Peng, Z., and K. Chao (2008), Non-volcanic tremor beneath the Central Range in Taiwan triggered by the 2001 *M_w* 7.8 Kunlun earthquake. *Geophys. J. Int.*, 175(2): 825–829.
- Peng, Z., and J. E. Vidale, (2008), Strong tremor near Parkfield, CA, excited by the 2002 Denali Fault earthquake, *Geophys. Res. Lett.*, 35(23): L23305.
- Ranero, C. R., R. von Huene, W. Weinrebe, and C. Reichert (2006), Tectonic processes along the Chile convergent margin, in *The Andes: Active Subduction Orogeny*, edited by O. Onken, et al., pp. 91–122, Berlin, Springer.
- Robertson Maurice, S. D., D. A. Wiens, K. D. Koper, and E. Vera, (2003), Crustal and upper mantle structure of southernmost South America inferred from regional waveform inversion, *J. Geophys. Res.*, 108(B1), 2038, doi:10.1029/2002JB001828.
- Rogers, G., and H. Dragert (2003), Episodic tremor and slip on the Cascadia subduction zone: The chatter of silent slip, *Science*, 20, 1492–1493.
- Rubinstein, J. L., and J. E. Vidale (2007), Non-volcanic tremor driven by large transient shear stresses, *Nature* 448(7153), 579–582.
- Rubinstein, J. L., M. La Rocca, J. E. Vidale, K. C. Creager, and A. G. Wech (2008), Tidal modulation of nonvolcanic tremor, *Science*, 319(5860), 186–189.
- Russo, R. M., A. Gallego, D. Comte, V. I. Mocanu, R. E. Murdie, and J. C. VanDecar (2010a), Source-side shear wave splitting and upper mantle flow in the Chile Ridge subduction region, *Geology*, 38(8), 707–710.
- Russo, R. M., J. C. VanDecar, D. Comte, V. I. Mocanu, A. Gallego, and R. E. Murdie (2010b), Subduction of the Chile Ridge: upper mantle structure and flow, *GSA Today*.
- Sánchez J. J., S. R. McNutt, J. A. Power, and M. Wyss (2004), Spatial variations in the frequency-magnitude distribution of earthquakes at Mt. Pinatubo volcano, *Bull. Seismol. Soc. Am.* 94:430–438.
- Scholz, C. H., (1968), The frequency-magnitude relation of microfracturing in rock and its relation to earthquakes, *Bull. Seismol. Soc. Am.*, 58, 1, 399–415.
- Shelly, D. R., G. C. Beroza, and S. Ide (2007a), Non-volcanic tremor and low-frequency earthquake swarms, *Nature*, 446 (7133), 305–307.
- Shelly, D. R., G. C. Beroza, and S. Ide (2007b), Complex evolution of transient slip derived from precise tremor locations in western Shikoku, Japan, *G-Cubed*, 8(10), 1525–2027.



- Shelly, D. R., G. C. Beroza, S. Ide, and S. Nakamura (2006), Low-frequency earthquakes in Shikoku, Japan, and their relationship to episodic tremor and slip, *Nature*, *442*, 188–191.
- Stein, R. S., G. C. P. King, and J. Lin (1994), Stress triggering of the 1994 $M=6.7$ Northridge, California, Earthquake by its predecessors, *Science*, *265*(5177), 1432–1435.
- Tebbens, S. F., G. K. Westbrook, S. C. Cande, S. D. Lewis, and N. L. Bangs (1990), Preliminary interpretation of combined GLORIA and SeaBeam imagery in the vicinity of the Chile margin triple junction, *Am. Assoc. Petrol. Geol.*, *74*, 776.
- Thomas, A. M., R. M. Nadeau, and R. Burgmann (2009), Tremor-tide correlations and near-lithostatic pore pressure on the deep San Andreas fault, *Nature*, *462*, 1048–1105.
- Tolstoy, M., F. L. Vernon, J. A. Orcutt, and F. K. Wyatt (2002), Breathing of the seafloor: Tidal correlations of seismicity at Axial volcano, *Geology*, *30*(6), 503–506.
- Wahr, J. (1995), *Earth Tides, Global Earth Physics, A Handbook of Physical Constants*, AGU Washington, DC., Reference Shelf, 40–46.
- Watanabe, T., Y. Hiramatsu, and K. Obara (2007), Scaling relationship between the duration and the amplitude of non-volcanic deep low-frequency tremors, *Geophys. Res. Lett.*, *34*, L07305.
- Wyss, M. (1973), Towards a physical understanding of the earthquake frequency distribution, *Geophys. J. R. Astron. Soc.* *31*, 341–359.
- Zahel, W. (1997). *Ocean Tides*, in *Lecture Notes in Earth Sciences 66*, edited by T. Phenomena, H. Wilhelm, W. Zürn, and H.-G. Wenzel, Springer Verlag, 398 pp.
- Zahel, W., J. Gavino, and U. Seiler (2000), Balances de Energia y Momento Angular de un Modelo Global de Mareas con Asimilación de Datos, *GEOS*, *20*(4), 400–413.